NANO · MICRO small
www.small-journal.com

Functionalized Fullerene for Inhibition of SARS-CoV-2 Variants

*Taylor M. Page, Chuanxiong Nie, Lenard Neander, Tatyana L. Povolotsky, Anil Kumar Sahoo, Philip Nickl, Julia M. Adler, Obida Bawadkji, Jörg Radnik, Katharina Achazi, Kai Ludwig, Daniel Lauster, Roland R. Netz, Jakob Trimpert, Benedikt Kaufer, Rainer Haag, and Ievgen S. Donskyi**

As virus outbreaks continue to pose a challenge, a nonspecific viral inhibitor can provide significant benefits, especially against respiratory viruses. Polyglycerol sulfates recently emerge as promising agents that mediate interactions between cells and viruses through electrostatics, leading to virus inhibition. Similarly, hydrophobic C_{60} fullerene can prevent virus infection via interactions with hydrophobic cavities of surface proteins. Here, two strategies are combined to inhibit infection of SARS-CoV-2 variants in vitro. Effective inhibitory concentrations in the millimolar range highlight the significance of bare fullerene's hydrophobic moiety and electrostatic interactions of polysulfates with surface proteins of SARS-CoV-2. Furthermore, microscale thermophoresis measurements support that fullerene linear polyglycerol sulfates interact with the SARS-CoV-2 virus via its spike protein, and highlight importance of electrostatic interactions within it. All-atom molecular dynamics simulations reveal that the fullerene binding site is situated close to the receptor binding domain, within 4 nm of polyglycerol sulfate binding sites, feasibly allowing both portions of the material to interact simultaneously.

1. Introduction

The COVID-19 pandemic caused by the SARS-CoV-2 virus persists as a public health crisis around the world. SARS-CoV-2 infected more than 600 million people, leading to the death of more than 6.5 million people.[1] Despite vaccination and public health measures taken, variants of concern continue to emerge.[2–4] Due to their proof-reading activity during viral genome replication,[5] coronaviruses typically mutate slower than other RNA viruses. However, more transmissible variants emerged including B.1.617.2/Delta,[6,7] B.1.1/Omicron,[8–10] and B.A.4/5[11] which efficiently spread in waves,[12–14] where latter variants that efficiently evaded wild-type vaccine immunity.[15–17] Thus, developing broad spectrum antiviral agents against respiratory viruses would be immensely valuable for the ongoing COVID-19 and future pandemics.

Viral surface proteins initiate infection by utilizing polyelectrolytic interactions, driven by counterion release,[18,19] in the glycocalyx for attachment to cellular glycans and glycoconjugates. When considering competitive inhibition, viral surfaces can act as a multivalent counterion for negatively charged polymers,[20] promoting virus–material interactions. To engage with receptors on host cells, many viruses utilize sulfated glycans such as heparan sulfate for initial attachment.[21–23]

T. M. Page, C. Nie, L. Neander, T. L. Povolotsky, P. Nickl, O. Bawadkji, K. Achazi, D. Lauster, R. Haag, I. S. Donskyi
Institut für Chemie und Biochemie
Freie Universität Berlin
Takustr. 3, 14195 Berlin, Germany
E-mail: ievgen.donskyi@fu-berlin.de

L. Neander, A. K. Sahoo, R. R. Netz
Physics Department
Freie Universität Berlin
Arnimallee 14, 14195 Berlin, Germany

The ORCID identification number(s) for the author(s) of this article can be found under https://doi.org/10.1002/smll.202206154.

DOI: 10.1002/smll.202206154

A. K. Sahoo
Max Planck Institute of Colloids and Interfaces
Am Mühlenberg 1, 14476 Potsdam, Germany

P. Nickl, J. Radnik, I. S. Donskyi
BAM – Federal Institute for Material Science and Testing
Division of Surface Analysis and Interfacial Chemistry
Unter den Eichen 44–46, 12205 Berlin, Germany

J. M. Adler, J. Trimpert, B. Kaufer
Institut für Virologie
Freie Universität Berlin
Robert-von-Ostertag-Straße 7, 14163 Berlin, Germany

J. M. Adler, J. Trimpert, B. Kaufer
Tiermedizinischen Zentrum für Resistenzforschung (TZR)
Freie Universität Berlin
14163 Berlin, Germany

K. Ludwig
Forschungszentrum für Elektronenmikroskopie and Core Facility
BioSupraMol
Freie Universität Berlin
Fabeckstraße 36A, 14195 Berlin, Germany

Heparin-like compounds have been developed into a variety of motifs for viral inhibition.[24–26] However, heparin and heparin analogs are limited in application due to their anticoagulant effects.[27–29] A synthetic alternative is sulfated polyglycerol, an anionic-based system, which is highly biocompatible[30] and has previously been investigated for antiviral applications.[30–34] Intriguingly, polyglycerol sulfates exhibit lower anticoagulant activity than heparin,[34] while remaining effective against heparan-sulfate binding viruses.[31,35] In addition, antiviral effects of anionic polymers have been investigated for various viruses that infect humans, in particular, sulfated polysaccharides display potent inhibitory properties against human immunodeficiency virus (HIV)[36–39] in vitro.[40] Particularly, dextran sulfate prevents infection of herpes simplex virus (HSV)[41] and HIV[42] by interacting with positively charged amino acids concentrated in the V3 region of HIV, which is important for binding to the host cell and subsequent fusion between viral and cell membranes.[43–45]

Further, SARS-CoV-2 spike (S) protein interacts specifically with cellular heparan sulfate.[46] The interaction between the S protein and heparan sulfate is understood to enhance the receptor-accessible "open" conformation of the receptor binding domain (RBD),[47] leading to successful angiotensin converting enzyme-2 (ACE-2) binding.[48,49] When considering the structure of S, in the RBD is a cluster of positively charged amino acid residues adjacent to ACE-2 binding site.[46] Additionally, there is a network of hydrophilic interactions found on both RBD-ACE-2 interfaces consisting of 13 hydrogen bonds and two salt bridges.[50] Linear polyglycerol sulfates have been investigated and reported for their interaction with heparin binding viruses, and thus are understood to interact in an analogous fashion to heparin.[46] SARS-CoV-2 Delta (B.1.617.2) and Omicron (B.1.1.529) variants have also has been shown to strongly attract lPGS.[51]

This hydrophilic network is in close proximity to a highly conserved threonine motif, suggesting it is significant for ACE-2 binding.[52] Further, Pokhrel, et al. discuss a conserved region between residues 541 and 612.[53] 12 positions are entirely invariable and 62% of the amino acid positions have two or fewer variations, when 441 168 individual virus sequences were examined.[53] However, the function of this region remains unknown. This conserved region is relatively hydrophobic and solvent exposed, composing part of the largest hydrophobic patch on the protein with a surface area of 370 Å^2. Additionally, the conserved hydrophobic patch is 81% identical to that on SARS-CoV-1 S protein, suggesting it maintains structural significance while being a potential target. Due to the hydrophobic nature of this region, mediating interactions with an ionic species alone is not feasible. Fullerene is an ≈1 nm spherical carbon allotrope that bears a hydrophobic surface and has been employed in carbon nanomaterials for a multitude of applications ranging from conductor integration and photovoltaics to biomedical applications.[54–58] Notably, it has been investigated against viruses such as Ebola,[59] influenza,[60] HSV,[61] and HIV.[62]

In this work, interactions of synthesized water-soluble fullerene derivatives with SARS-CoV-2 are investigated to assess their inhibitory properties. Our data highlight the significant antiviral activity of a fullerene linear polyglycerol sulfate. Moreover, we examine controls and precursors to support the significance of each feature's role in viral inhibition. Docking studies performed and followed by all-atom molecular dynamics simulations in explicit solvent, identify the possible fullerene binding site on the S protein, and is further supported by microscale thermophoresis (MST).

2. Results and Discussion

Interactions between viruses and sulfated linear polyglycerol fullerene derivatives are investigated for their antiviral effects. Beginning with pristine fullerene, the pyramidalization of the sp^2 carbon atoms creates a strain energy, which is a driving force for the nitrene [2+1] cycloaddition reaction (**Figure 1**).[63] Following fullerene's functionalization with dichlorotriazine, a block copolymer of linear polyglycerol and cysteamine-modified poly(allyl glycidyl ether) (PAGE, 10%) (lPG) is conjugated through nucleophilic aromatic substitution at ambient temperature. Finally, the viable hydroxyl groups of lPG are sulfated with sulfamic acid. Each synthetic step is monitored by X-ray photoelectron spectroscopy (XPS) and near-edge X-ray adsorption fine structure (NEXAFS) spectroscopy, and further supported by zeta-potential measurements, and thermal and elemental analysis (**Figure 2**). First, from the highly resolved C 1s XP spectrum of fullerene-triazine (FT), the major chemical state is found at 285 eV corresponding to $C_{sp2/sp3}$ and in the binding energy regime between 286.1 and 288.6 eV where the typical shoulder with chemical states corresponding to triazine components is found[64–66] (Figure 2a and Table S1, Supporting Information). Moreover, a highly resolved N 1s XP spectrum

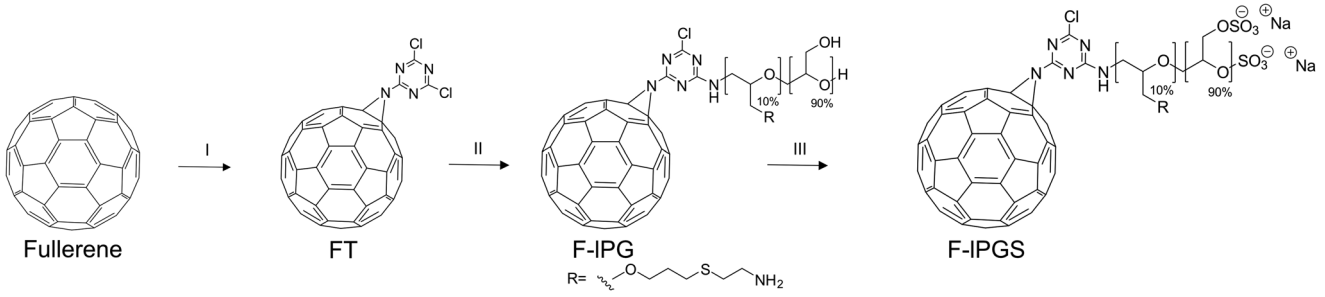

Figure 1. Schematic representation of fullerene-linear polyglycerol b-amine sulfate synthesis (F-lPGS). I) Cyanuric chloride, sodium azide, acetone/dimethylformamide, 24 h, 0–25 °C. II) lPG, dimethylformamide, triethylamine, 24 h, 25 °C. III) Sulfamic acid, dimethylformamide, 24 h, 60 °C.

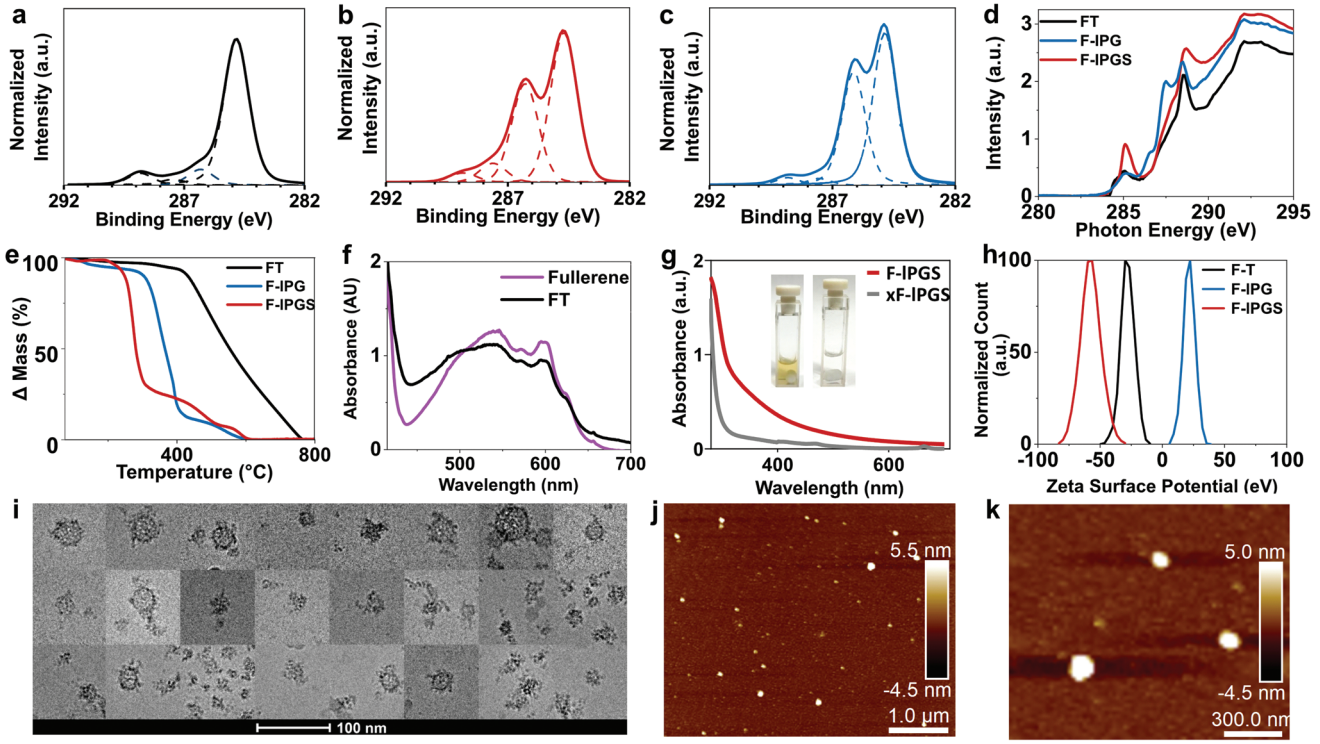

Figure 2. Highly resolved XPS C 1s spectra of a) FT, b) F-lPG, and c) F-lPGS. d) NEXAFS of FT, F-lPG, and F-lPGS, e) thermogravimetric analysis of FT, F-lPG, and F-lPGS. f) UV-vis absorbance of fullerene and FT, g) UV-vis absorbance of F-lPGS and xF-lPGS. h) Zeta surface potential of FT, F-lPG, and F-lPGS. i) Cryo-TEM image of F-lPGS agglomerates. j) AFM image of F-lPGS agglomerates, and k) zoomed-in AFM image of F-lPGS agglomerates.

shows two components at 398.0 and 399.6 eV, corresponding to different nitrogen species of the dichlorotriazine moieties, as seen in previously published results[32,67] (Figure S3b, Supporting Information). The C K-edge NEXAFS spectrum for FT is displayed in Figure 2a and Table S2 in the Supporting Information. At the low-energy side, the NEXAFS spectrum shows a sharp resonance at a photon energy of 285.1 eV corresponding to the C 1s → π^* transition.[68–70] In the "fingerprint" region between 286 and 290 eV, a new resonance occurs (*b*) which is related to a conjugation of triazine to fullerene by a C—N bond. Similar resonances have been found before for triazine molecules conjugated to other carbon materials such as thermally reduced graphene oxide.[71] Here, π^* and σ^* refer to antibonding molecular orbital states of π and σ symmetries, respectively. The resonance *b* in the finger-print region for FT shifts upward of π^* states and transitions from the fullerene carbon C 1s orbital to unoccupied molecular orbitals of the conjugated triazine moiety. Thermogravimetric analysis is also used to support fullerene modification where roughly 15% of mass loss is observed at 500 °C. Time-of-flight secondary ion mass spectrometry spectrum of FT supports the presence of the fullerene moiety (Figure S4, Supporting Information). A noticeable shift in elemental analysis (**Table 1**) supports the modification of the fullerene surface with one dichlorotriazine functional group and a color shift is observed, characterized by UV-vis spectroscopy and corresponding change in solubility resulting in a shift in the surface charge (Figure 2h).

The block co-polymer, lPG, is conjugated at ambient temperature [72,73] through nucleophilic aromatic substitution of one chlorine atom of the dichlorotriazine moieties mechanism (Figure 1) resulting in a water-soluble product that is isolated through centrifugation. The thermogram (Figure 2e) indicates over 90% mass loss due to PG decomposition prior to 450 °C. This also corresponds to C—O bonds in the highly resolved C 1s XP spectra of F-lPG and F-lPGS (Figure 2b,c), as well as the appearance of resonances *c*, *d*, and *e* in C K-edge NEXAFS (Figure S3d, Supporting Information) which supports successful conjugation. Sulfation reactions are conducted with sulfamic acid and F-lPG, fullerene dendritic polyglycerol (F-dPG), and a fullerene absent control lPG, resulting in highly sulfated polymers. To monitor the change in mass, gel permeation chromatography shows an increase in the average molecular

Table 1. Characterization of fullerene derivatives starting from pristine fullerene, with elemental analysis and zeta potential values taken at 1.0 mg mL^{-1}.

COMPOUND	C [%]	H [%]	N [%]	S [%]	ZETA-POTENTIAL [MV]
FULLERENE	98.8	1.8	0.0	0.0	n.a.
FT	91.2	0.4	4.3	0.0	–28.0 ± 5.2
LPG	45.7	8.5	7.8	0.0	+27.5 ± 2.6
LPGS	29.2	5.5	0.7	9.3	–31.9 ± 19.7
F-LPG	46.9	7.7	0.8	0.7	+21.5 ± 4.7
F-DPGS	20.2	3.0	0.1	18.0	–49.4 ± 9.3
F-LPGS	23.1	5.7	6.0	16.7	–51.9 ± 16.4

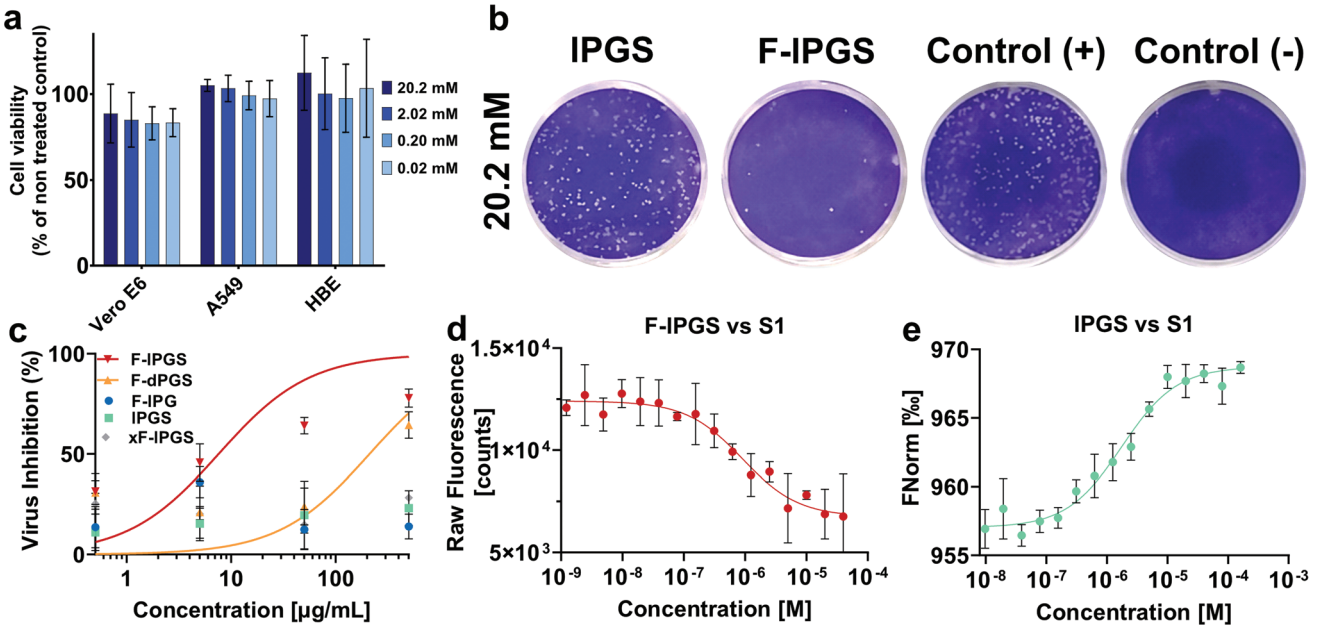

Figure 3. a) The cytotoxicity of different derivatives and precursors are investigated using three cell lines Vero E6, A549, and 16HBE14o- (HBE) ($n = 3$, mean with SD). b) Comparison of inhibitors against SARS-CoV-2 (WT) infection in a plaque reduction assay at 20.2×10^{-3} M (500 µg mL^{-1}) on Vero E6 cells. c) Results of plaque reduction assays using Vero E6 cells for IC_{50} determination of different compounds against SARS-CoV-2 WT ($n = 4$). Microscale thermophoresis measurements of d) F-lPGS against spike S1+S2 ECD-His and e) lPGS against spike S1+S2 ECD-His. Data points fitted with one sited fit assuming a 1:1 ligand to receptor ratio.

weight from 10.0 to 24.7 kDa, which when cross-analyzed with elemental analysis determines F-lPGS to be a 95% degree of sulfation (Equation (S2), Supporting Information), along with a shift in zeta surface potential from 21.5 ± 4.7 eV of F-lPG to −51.9 ± 16.4 eV after sulfation (Table 1). Microscopy, through cryo-transmission electron microscopy (cryo-TEM) and atomic force microscopy (AFM, Figure 2i–k), also shows formation of relatively homogenous agglomerates between 20–50 and 100 nm in diameter, respectively, largely driven by the hydrophobic interactions between fullerene molecules.

Cell viability assays performed at various dilutions using cell counting kit-adenocarcinomic human alveolar basal epithelial cells (A549), human bronchial epithelial cells (HBE), and kidney epithelial cells from African green monkeys (Chlorocebus) (Vero E6) examine F-lPGS, alongside lPGS and F-lPG, and sodium dodecyl sulfate as a positive toxic control (**Figure 3**b and Figures S8–S10, Supporting Information). A549 cells and 16HBE14o- cells are alveolar type II cell,[74,75] thus representing analogous cells that this material is attempting to protect, and accounts for the pulmonary surfactant. Vero E6 cells are particularly important because they do not produce interferon alpha or beta, which stimulate antiviral defenses of nearby cells and are a standard model cell line for virus infection studies.[76] Resulting cell viability studies reveal no significant toxicity within the examined plaque reduction assay concentrations of 0.02×10^{-3} and 20.2×10^{-3} M, providing an EC_{50} of 70.2×10^{-3} M against Vero E6 cells (Figure S11, Supporting Information). Viral inhibitory activity against two SARS-CoV-2 variants of the synthesized materials is evaluated in vitro on Vero E6 cells using plaque reduction assays. First, lPGS is compared with F-lPGS for its inhibitory activity against wild-type SARS-CoV-2 (Figure 3b and Figure S7, Supporting Information). However, lPGS does not show inhibitory activity, probably because its molecular weight is too low (10 kDa), when compared to other sulfated linear polyglycerol inhibitors, 40 kDa lPGS provides an IC_{50} of 67 mg mL^{-1} (≈1.6×10^{-3} M),[77] to block the viral interaction with the host cells alone. To investigate the structural role of the fullerene-based inhibitors, F-dPG, F-dPGS, F-lPG, F-lPGS, and xF-lPGS are compared with the same assay and their half-maximal inhibition concentration (IC_{50}) are determined as shown in Figure 3c. Only two materials show inhibitory activity within the examined concentration range: F-lPGS and F-dPGS, which display an IC_{50} of 0.32×10^{-3} and 8.51×10^{-3} M against the wild type, respectively. The resulting selectivity index for F-lPGS is 220.7 which for antiviral agents is promising for further examination.[78,79] Comparing F-lPGS to F-dPGS emphasizes the greater efficacy of lPGS due to its ability to span greater distances and conform to positively charged pockets. A further control to highlight the important role bare fullerene play is produced by photocrosslinking fullerene through a [2 + 2] cycloaddition.[80,81] A solution of F-lPGS reacts under UV-light for 24 h, resulting in a colorless solution of crosslinked F-lPGS (xF-lPGS), which displays no inhibitory activity, in comparison to the yellow-brown solution of F-lPGS (Figure 2g), due to the hindrance of a single fullerene's ability to interact with S. Therefore, when considering controls, the significance of each part—the anionic sulfated polymer chain and bare fullerene—working in tandem is clear with a substantial drop in inhibition after fullerene is photocrosslinked. F-lPGS is further tested against SARS-CoV-2 omicron BA.5 variant, as observed in a quantitative polymerase chain reaction-based pre-infection assay using fluorescence

labeling (Figure S6, Supporting Information). The results show IC_{50} between 2.02×10^{-3} and 0.20×10^{-3} M.

To understand the possible binding mechanisms, MST is used to determine the binding affinities (K_d-values) for F-lPGS and spike S1+S2 ECD-His (K_d 881.9×10^{-9} M), lPGS and spike S1+S2 ECD-His (K_d 1.7×10^{-6} M), and lPGS and spike RBD-His (K_d 15×10^{-6} M) (Table S5, Supporting Information). lPGS binds to both RBD and S1 domains of the spike protein in the micromolar range. Further, no binding can be determined until 40×10^{-6} M between F-lPGS and RBD. However, F-lPGS and S1 have the highest binding affinities of $881.9 \pm 201.1 \times 10^{-9}$ M, further supporting the hypothesis that fullerene binds to the conserved hydrophobic region in the S1 domain of the spike protein (Figure 3e), while lPGS binds to the cationic patch on the RBD (Figure S12, Supporting Information).

To further explore possible binding sites of fullerene, docking studies are performed followed by explicit solvent all-atom molecular dynamics (MD) simulations (see the Supporting Information). Previous simulations have been conducted to illustrate potential targets and docking sites of fullerene and carbon nanotubes against SARS-CoV-2 similar to currently prescribed drugs,[82] that perturb the electrostatic characteristic of the binding site.[83] To make simulations feasible despite the large size of the spike protein trimer, only residues 290–705 of one spike protein monomer in the open conformation are taken (see **Figure 4**a). This portion of the protein contains the RBD (Figure 4b, RBD in red), where lPGS shows strong binding to the cationic patch (see the electrostatic potential map in Figure S13, Supporting Information).[77] Furthermore, the chosen structure contains the conserved region (residues 541–612) with the largest hydrophobic patch (Figure 4b, green residues).[53] The conserved region might be a possible binding site for fullerene due to its hydrophobic character. Docking studies with a fullerene molecule show three different potential binding sites (see yellow, purple, and cyan fullerene molecules in Figure 4b). But only one of these three binding sites is solvent accessible in the trimeric conformation of the spike protein (Figure 4b, cyan fullerene). This binding site is located in between the conserved region and the RBD. It also has the lowest interaction energy from docking (−4.27 kcal mol^{-1}) and is therefore more promising than the other docking sites. Additional simulations with lPGS-22mer, fullerene, and F-lPGS for residues 290 to 705 of the spike protein (Figures S14 and S15, Supporting Information), which support that lPGS interacts with the S protein, as observed in MST.

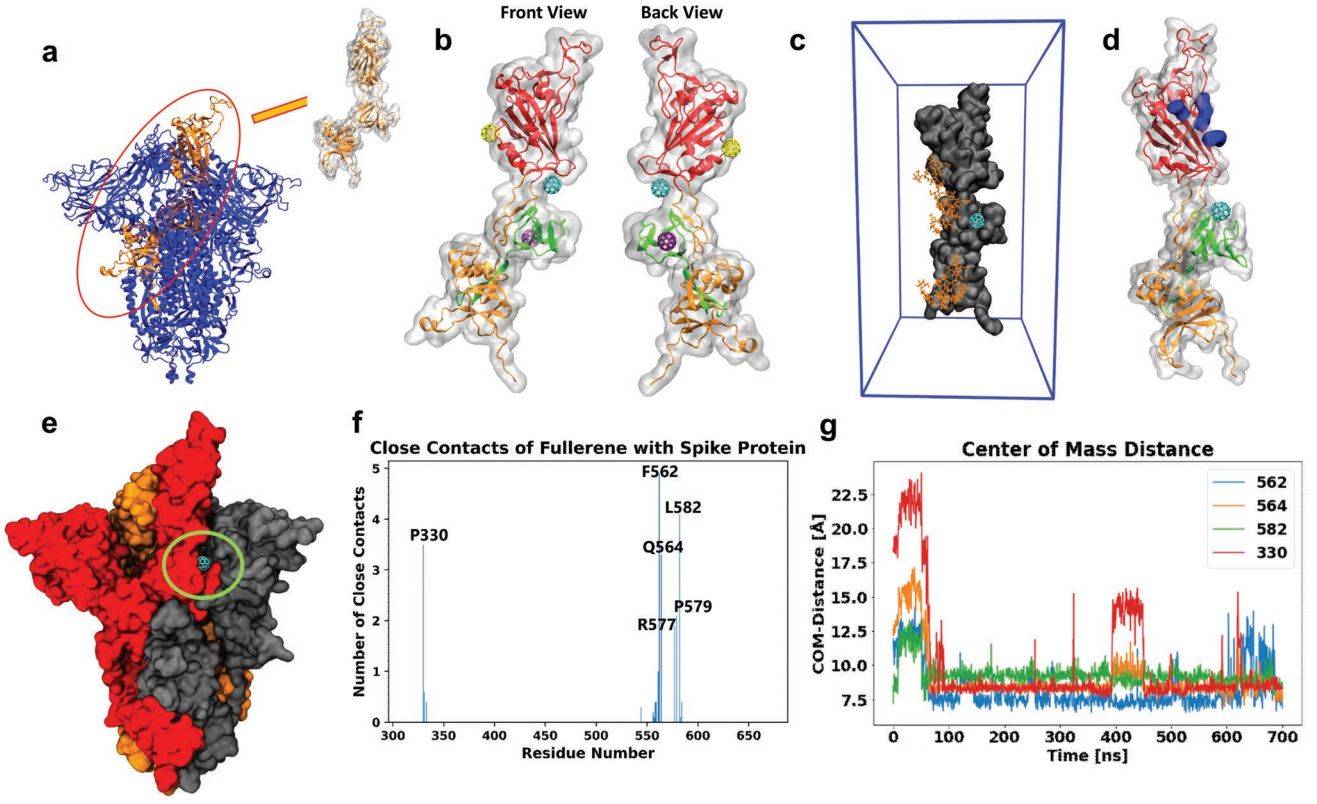

Figure 4. a) Residues 290–705 (orange) of one spike protein monomer in the open conformation are used for docking studies and all-atom MD simulations (spike protein trimer in blue). b) Observed binding sites from docking studies for fullerene, only the cyan fullerene position is accessible in the trimeric conformation. This binding site is located between the RBD (red) and the conserved region (green). c) MD simulation set-up, starting position of fullerene in cyan, glycans in orange. Water and ions are not shown for clarity. d) Final adsorption position of fullerene (cyan) after 700 ns simulation. The final position is situated on the conserved region (green) and is ≈4 nm away from the cationic patch on the RBD (blue residues). e) Final adsorption position of the fullerene (cyan, indicated by a circle) is solvent accessible in the trimeric conformation of the spike protein (monomers in red, gray, and orange). f) Close contacts of fullerene with the spike protein observed in the 700 ns simulation. g) Time evolution of the center-of-mass distance between fullerene and different residues with a greater number of close contacts.

An MD simulation, conducted for 700 ns with the fullerene placed at the conserved region as a starting position (Figure 4c), results in the fullerene molecule residing in a region close to the identified site in the docking study. Residues with a greater number of close contacts with fullerene are found to be highly hydrophobic (F562 and L582, see Figure 4f). The observed binding site is also solvent accessible for every monomer of the trimeric spike protein, whether the RBD is in the open or closed conformation (see Figure 4e and Figure S13, Supporting Information). Once fullerene binds to the binding site, it stays there for the remaining time of the simulation (Figure 4g). This implies that the relaxation times are in the order of microseconds or more. Transferring the MD results to the experimentally studied F-lPGS conjugates, it is plausible that these conjugates strongly interact with the spike protein in a bivalent manner. First, fullerene binds to the conserved, hydrophobic region while lPGS (10 kDa), with a contour length of 40 nm, binds to the cationic patch on the RBD which is ≈4 nm away from the fullerene binding site (see Figure 4d). Through MST measurements, we support that F-lPGS specifically binds to a region outside the binding domain with a K_d of $881.0 \pm 201.1 \times 10^{-9}$ M. When compared directly to its fullerene free analog lPGS, it was observed that it had half the binding affinity, and further showed a binding affinity to the RBD, while F-lPGS did not.

3. Conclusion

In summary, the novel synergistic effects of combining fullerene with highly sulfated lPG renders an effective antiviral SARS-CoV-2 agent. lPGS's ability to conform to the surface protein's positive charges is highlighted through MST measurements of both lPGS and F-lPGS. Further, simulations support that fullerene interacts with residues on a hydrophobic patch with a currently unknown but potentially significant implications, with close proximity to the RBD. The novel presentation of our findings supports the importance of the addition of fullerene to lPGS to inhibit SARS-CoV-2, predicted by simulation/docking studies, and supported by MST through nonspecific interactions on the spike protein. In the end, synthesized F-lPGS displays high potency against different variants of SARS-CoV-2 as shown using various virus inhibition assays.

Supporting Information

Supporting Information is available from the Wiley Online Library or from the author.

Acknowledgements

The authors would like to thank Daniel Kutifa for his support in polymer synthesis, Elisa Quaas for her support in toxicological assays, and M. Eng. Jörg Stockmann from BAM 6.1 for his support with XPS data acquisition. The authors want to thank Dr. Victor M. Corman, Dr. Daniela Niemeyer, Prof. Dr. Christian Drosten, Prof. Dr. Chantal Reusken, Dr. Daniel Bourquain and European Virus Archive GLOBAL (EVAg) for providing the viruses used in this study. VeroE6-TMPRSS cells were provided by the NIBSC Research Reagent Repository, UK, with thanks to Dr. Makoto Takeda. The authors acknowledge financial support by the DFG-funded International Research Training Group GRK2662 and Berlin University Alliance (BUA). The authors would also like to thank Prof. Dr. Mohsen Adeli, Prof. Dr. Andreas Hermann for their continuous support. J.T. acknowledges support by the European Union's Horizon 2020 research and innovation program - EVA-GLOBAL grant 871029. A.K.S. and R.R.N. acknowledge support from the Max-Planck MaxWater initiative. R.H. acknowledges the financial support from the ERC advanced grant SupraVir. I.D. acknowledges the Federal Ministry of Education and Research (BMBF) in the framework of NanoMatFutur (PathoBlock) for financial support (project number 13XP5191). D.L. acknowledges funding by the Federal Ministry of Education and Science (BMBF; grant number: 13XP5111), and we further thank for support from the SupraFAB research building realized with funds from the federal government and the city of Berlin.

Open access funding enabled and organized by Projekt DEAL.

Conflict of Interest

The authors declare no conflict of interest.

Data Availability Statement

The data that support the findings of this study are available from the corresponding author upon reasonable request.

Keywords

covalent functionalization, fullerene, SARS-CoV-2, sulfated materials, virus inhibition

Received: October 7, 2022
Revised: December 25, 2022
Published online: January 18, 2023

[1] WHO Coronavirus (COVID-19) Dashboard | WHO Coronavirus (COVID-19) Dashboard With Vaccination Data, https://covid19.who.int/ (accessed: October 2022).
[2] T. Kustin, N. Harel, U. Finkel, S. Perchik, S. Harari, M. Tahor, I. Caspi, R. Levy, M. Leschinsky, S. K. Dror, G. Bergerzon, H. Gadban, F. Gadban, E. Eliassian, O. Shimron, L. Saleh, H. Ben-Zvi, E. K. Taraday, D. Amichay, A. Ben-Dor, D. Sagas, M. Strauss, Y. S. Avni, A. Huppert, E. Kepten, R. D. Balicer, D. Nezer, S. Ben-Shachar, A. Stern, *Nat. Med.* **2021**, *27*, 1379.
[3] H. Tegally, E. Wilkinson, M. Giovanetti, A. Iranzadeh, V. Fonseca, J. Giandhari, D. Doolabh, S. Pillay, E. J. San, N. Msomi, K. Mlisana, A. von Gottberg, S. Walaza, M. Allam, A. Ismail, T. Mohale, A. J. Glass, S. Engelbrecht, G. van Zyl, W. Preiser, F. Petruccione, A. Sigal, D. Hardie, G. Marais, N. yuan Hsiao, S. Korsman, M. A. Davies, L. Tyers, I. Mudau, D. York, et al., *Nature* **2021**, *592*, 438.
[4] N. R. Faria, T. A. Mellan, C. Whittaker, I. M. Claro, D. D. S. Candido, S. Mishra, M. A. E. Crispim, F. C. S. Sales, I. Hawryluk, J. T. McCrone, R. J. G. Hulswit, L. A. M. Franco, M. S. Ramundo, J. G. de Jesus, P. S. Andrade, T. M. Coletti, G. M. Ferreira, C. A. M. Silva, E. R. Manuli, R. H. M. Pereira, P. S. Peixoto, M. U. G. Kraemer, N. Gaburo, C. D. C. Camilo, H. Hoeltgebaum, W. M. Souza, E. C. Rocha, L. M. de Souza, M. C. de Pinho, L. J. T. Araujo, et al., *Science* **2021**, *372*, 815.
[5] M. R. Denison, R. L. Graham, E. F. Donaldson, L. D. Eckerle, R. S. Baric, *RNA Biol.* **2011**, *8*, 270.

[6] D. Planas, D. Veyer, A. Baidaliuk, I. Staropoli, F. Guivel-Benhassine, M. M. Rajah, C. Planchais, F. Porrot, N. Robillard, J. Puech, M. Prot, F. Gallais, P. Gantner, A. Velay, J. le Guen, N. Kassis-Chikhani, D. Edriss, L. Belec, A. Seve, L. Courtellemont, H. Péré, L. Hocqueloux, S. Fafi-Kremer, T. Prazuck, H. Mouquet, T. Bruel, E. Simon-Lorière, F. A. Rey, O. Schwartz, *Nature* **2021**, *596*, 276.
[7] P. Mlcochova, S. Kemp, M. S. Dhar, G. Papa, B. Meng, I. A. T. M. Ferreira, R. Datir, D. A. Collier, A. Albecka, S. Singh, R. Pandey, J. Brown, J. Zhou, N. Goonawardane, S. Mishra, C. Whittaker, T. Mellan, R. Marwal, M. Datta, S. Sengupta, K. Ponnusamy, V. S. Radhakrishnan, A. Abdullahi, O. Charles, P. Chattopadhyay, P. Devi, D. Caputo, T. Peacock, D. C. Wattal, N. Goel, et al., *Nature* **2021**, *599*, 114.
[8] Y. Araf, F. Akter, Y. dong Tang, R. Fatemi, M. S. A. Parvez, C. Zheng, M. G. Hossain, *J. Med. Virol.* **2022**, *94*, 1825.
[9] R. Viana, S. Moyo, D. G. Amoako, H. Tegally, C. Scheepers, C. L. Althaus, U. J. Anyaneji, P. A. Bester, M. F. Boni, M. Chand, W. T. Choga, R. Colquhoun, M. Davids, K. Deforche, D. Doolabh, L. du Plessis, S. Engelbrecht, J. Everatt, J. Giandhari, M. Giovanetti, D. Hardie, V. Hill, N. Y. Hsiao, A. Iranzadeh, A. Ismail, C. Joseph, R. Joseph, L. Koopile, S. L. Kosakovsky Pond, M. U. G. Kraemer, et al., *Nature* **2022**, *603*, 679.
[10] L. Liu, S. Iketani, Y. Guo, J. F. W. Chan, M. Wang, L. Liu, Y. Luo, H. Chu, Y. Huang, M. S. Nair, J. Yu, K. K. H. Chik, T. T. T. Yuen, C. Yoon, K. K. W. To, H. Chen, M. T. Yin, M. E. Sobieszczyk, Y. Huang, H. H. Wang, Z. Sheng, K. Y. Yuen, D. D. Ho, *Nature* **2021**, *602*, 676.
[11] Q. Wang, Y. Guo, S. Iketani, M. S. Nair, Z. Li, H. Mohri, M. Wang, J. Yu, A. D. Bowen, J. Y. Chang, J. G. Shah, N. Nguyen, Z. Chen, K. Meyers, M. T. Yin, M. E. Sobieszczyk, Z. Sheng, Y. Huang, L. Liu, D. D. Ho, *Nature* **2022**, *608*, 603.
[12] K. Paniskaki, M. Anft, T. L. Meister, C. Marheinecke, S. Pfaender, S. Skrzypczyk, F. S. Seibert, C. J. Thieme, M. J. Konik, S. Dolff, O. Anastasiou, B. Holzer, U. Dittmer, C. Queren, L. Fricke, H. Rohn, T. H. Westhoff, O. Witzke, U. Stervbo, T. Roch, N. Babel, *Front. Immunol.* **2022**, *13*, 74.
[13] M. Bergwerk, T. Gonen, Y. Lustig, S. Amit, M. Lipsitch, C. Cohen, M. Mandelboim, E. G. Levin, C. Rubin, V. Indenbaum, I. Tal, M. Zavitan, N. Zuckerman, A. Bar-Chaim, Y. Kreiss, G. Regev-Yochay, *N. Engl. J. Med.* **2021**, *385*, 1474.
[14] E. Hacisuleyman, C. Hale, Y. Saito, N. E. Blachere, M. Bergh, E. G. Conlon, D. J. Schaefer-Babajew, J. DaSilva, F. Muecksch, C. Gaebler, R. Lifton, M. C. Nussenzweig, T. Hatziioannou, P. D. Bieniasz, R. B. Darnell, *N. Engl. J. Med.* **2021**, *384*, 2212.
[15] V. V. Edara, C. Norwood, K. Floyd, L. Lai, M. E. Davis-Gardner, W. H. Hudson, G. Mantus, L. E. Nyhoff, M. W. Adelman, R. Fineman, S. Patel, R. Byram, D. N. Gomes, G. Michael, H. Abdullahi, N. Beydoun, B. Panganiban, N. McNair, K. Hellmeister, J. Pitts, J. Winters, J. Kleinhenz, J. Usher, J. B. O'Keefe, A. Piantadosi, J. J. Waggoner, A. Babiker, D. S. Stephens, E. J. Anderson, S. Edupuganti, et al., *Cell Host Microbe* **2021**, *29*, 516.
[16] W. Dejnirattisai, D. Zhou, P. Supasa, C. Liu, A. J. Mentzer, H. M. Ginn, Y. Zhao, H. M. E. Duyvesteyn, A. Tuekprakhon, R. Nutalai, B. Wang, C. López-Camacho, J. Slon-Campos, T. S. Walter, D. Skelly, S. A. Costa Clemens, F. G. Naveca, V. Nascimento, F. Nascimento, C. Fernandes da Costa, P. C. Resende, A. Pauvolid-Correa, M. M. Siqueira, C. Dold, R. Levin, T. Dong, A. J. Pollard, J. C. Knight, D. Crook, T. Lambe, et al., *Cell* **2021**, *184*, 2939.
[17] F. Amanat, S. Strohmeier, P. Meade, N. Dambrauskas, B. Mühlemann, D. J. Smith, V. Vigdorovich, D. Noah Sather, L. Coughlan, F. Krammer, *PLoS Biol.* **2021**, *19*, e3001384.
[18] M. T. Record, C. F. Anderson, T. M. Lohman, *Q. Rev. Biophys.* **1978**, *11*, 103.
[19] X. Xu, Q. Ran, P. Dey, R. Nikam, R. Haag, M. Ballauff, J. Dzubiella, *Biomacromolecules* **2018**, *19*, 409.
[20] K. Achazi, R. Haag, M. Ballauff, J. Dernedde, J. N. Kizhakkedathu, D. Maysinger, G. Multhaup, *Angew. Chem., Int. Ed.* **2021**, *60*, 3882.
[21] V. Tiwari, E. Maus, I. M. Sigar, K. H. Ramsey, D. Shukla, *Glycobiology* **2012**, *22*, 1402.
[22] M. Koehler, M. Delguste, C. Sieben, L. Gillet, D. Alsteens, *Annu. Rev. Virol.* **2020**, *7*, 143.
[23] V. Cagno, E. D. Tseligka, S. T. Jones, C. Tapparel, *Viruses* **2019**, *11*, 596.
[24] F. Schandock, C. F. Riber, A. Röcker, J. A. Müller, M. Harms, P. Gajda, K. Zuwala, A. H. F. Andersen, K. B. Løvschall, M. Tolstrup, F. Kreppel, J. Münch, A. N. Zelikin, *Adv. Healthcare Mater.* **2017**, *6*, 1700748.
[25] R. H. Bianculli, J. D. Mase, M. D. Schulz, *Macromolecules* **2020**, *53*, 9158.
[26] P. Dey, T. Bergmann, J. L. Cuellar-Camacho, S. Ehrmann, M. S. Chowdhury, M. Zhang, I. Dahmani, R. Haag, W. Azab, *ACS Nano* **2018**, *12*, 6429.
[27] I. Ahmed, A. Majeed, R. Powell, *Postgrad. Med. J.* **2007**, *83*, 575.
[28] K. D. Murphy, D. H. Galla, C. J. Vaughn, G. McCrohan, W. J. Garrisi, *Radiographics* **1998**, *18*, 111.
[29] Q. Ma, B. Dudas, A. Daud, O. Iqbal, D. Hoppensteadt, W. Jeske, U. Cornelli, J. Lee, S. Lorens, R. Mervis, I. Hanin, I. Capila, R. Linhardt, J. Fareed, *Thromb. Res.* **2002**, *105*, 303.
[30] M. Bochenek, N. Oleszko-Torbus, W. Wałach, D. Lipowska-Kur, A. Dworak, A. Utrata-Wesołek, *Polym. Rev.* **2020**, *60*, 717.
[31] J. Vonnemann, C. Sieben, C. Wolff, K. Ludwig, C. Böttcher, A. Herrmann, R. Haag, *Nanoscale* **2014**, *6*, 2353.
[32] I. S. Donskyi, W. Azab, J. L. Cuellar-Camacho, G. Guday, A. Lippitz, W. E. S. Unger, K. Osterrieder, M. Adeli, R. Haag, *Nanoscale* **2019**, *11*, 15804.
[33] H. Türk, R. Haag, S. Alban, *Bioconjugate Chem.* **2004**, *15*, 162.
[34] P. Pouyan, C. Nie, S. Bhatia, S. Wedepohl, K. Achazi, N. Osterrieder, R. Haag, *Biomacromolecules* **2021**, *22*, 1545.
[35] I. Papp, C. Sieben, A. L. Sisson, J. Kostka, C. Böttcher, K. Ludwig, A. Herrmann, R. Haag, *ChemBioChem* **2011**, *12*, 887.
[36] M. Witvrouw, E. de Clercq, *Gen. Pharmacol.* **1997**, *29*, 497.
[37] N. Koizumi, H. Sakagami, A. Utsumi, S. Fujinaga, M. Takeda, K. Asano, I. Sugawara, S. Ichikawa, H. Kondo, S. Mori, K. Miyatake, Y. Nakano, H. Nakashima, T. Murakami, N. Miyano, N. Yamamoto, *Antiviral Res.* **1993**, *21*, 1.
[38] E. Sanniyasi, G. Venkatasubramanian, M. M. Anbalagan, P. P. Raj, R. K. Gopal, *Sci. Rep.* **2019**, *9*, 12185.
[39] V. H. Pomin, F. F. Bezerra, P. A. G. Soares, *Curr. Pharm. Des.* **2017**, *23*, 3405.
[40] M. Ito, M. Baba, A. Sato, R. Pauwels, E. de Clercq, S. Shigeta, *Antiviral Res.* **1987**, *7*, 361.
[41] M. Baba, R. Pauwels, J. Balzarini, J. Arnout, J. Desmyter, E. de Clercq, *Proc. Natl. Acad. Sci. U. S. A.* **1988**, *85*, 6132.
[42] H. Mitsuya, D. J. Looney, S. Kuno, R. Ueno, F. Wong-Staal, S. Broder, *Science* **1988**, *240*, 646.
[43] L. N. Callahan, M. Phelan, M. Mallinson, M. A. Norcross, *J. Virol.* **1991**, *65*, 1543.
[44] D. Batinic, F. A. Robey, *J. Biol. Chem.* **1992**, *267*, 6664.
[45] D. Schols, R. Pauwels, J. Desmyter, E. de Clercq, *Virology* **1990**, *175*, 556.
[46] T. M. Clausen, D. R. Sandoval, C. B. Spliid, J. Pihl, H. R. Perrett, C. D. Painter, A. Narayanan, S. A. Majowicz, E. M. Kwong, R. N. McVicar, B. E. Thacker, C. A. Glass, Z. Yang, J. L. Torres, G. J. Golden, P. L. Bartels, R. N. Porell, A. F. Garretson, L. Laubach, J. Feldman, X. Yin, Y. Pu, B. M. Hauser, T. M. Caradonna, B. P. Kellman, C. Martino, P. L. S. M. Gordts, S. K. Chanda, A. G. Schmidt, K. Godula, et al., *Cell* **2020**, *183*, 1043.

[47] D. Wrapp, N. Wang, K. S. Corbett, J. A. Goldsmith, C.-L. Hsieh, O. Abiona, B. S. Graham, J. S. Mclellan, *Science* **2020**, *367*, 1260.
[48] A. C. Walls, Y. J. Park, M. A. Tortorici, A. Wall, A. T. McGuire, D. Veesler, *Cell* **2020**, *181*, 281.
[49] J. Yang, S. J. L. Petitjean, M. Koehler, Q. Zhang, A. C. Dumitru, W. Chen, S. Derclaye, S. P. Vincent, P. Soumillion, D. Alsteens, *Nat. Commun.* **2020**, *11*, 4541.
[50] J. Lan, J. Ge, J. Yu, S. Shan, H. Zhou, S. Fan, Q. Zhang, X. Shi, Q. Wang, L. Zhang, X. Wang, *Nature* **2020**, *581*, 215.
[51] C. Nie, A. Kumar Sahoo, R. R. Netz, A. Herrmann, M. Ballauff, R. Haag, *ChemBioChem* **2022**, *23*, 202100681.
[52] W. Li, C. Zhang, J. Sui, J. H. Kuhn, M. J. Moore, S. Luo, S. K. Wong, I. C. Huang, K. Xu, N. Vasilieva, A. Murakami, Y. He, W. A. Marasco, Y. Guan, H. Choe, M. Farzan, *EMBO J.* **2005**, *24*, 1634.
[53] S. Pokhrel, B. R. Kraemer, S. Burkholz, D. Mochly-Rosen, *Sci. Rep.* **2021**, *11*, 13120.
[54] F. Diederich, M. Gómez-López, *Chem. Soc. Rev.* **1999**, *28*, 263.
[55] M. Bendikov, F. Wudl, D. F. Perepichka, *Chem. Rev.* **2004**, *104*, 4891.
[56] H. Imahori, S. Fukuzumi, *Adv. Funct. Mater.* **2004**, *14*, 525.
[57] L. Gan, S. Huang, X. Zhang, A. Zhang, B. Cheng, H. Cheng, X. Li, G. Shang, *J. Am. Chem. Soc.* **2002**, *124*, 13384.
[58] S. Bosi, T. da Ros, G. Spalluto, M. Prato, *Eur. J. Med. Chem.* **2003**, *38*, 913.
[59] A. Muñoz, D. Sigwalt, B. M. Illescas, J. Luczkowiak, L. Rodríguez-Pérez, I. Nierengarten, M. Holler, J.-S. Remy, K. Buffet, S. P. Vincent, J. Rojo, R. Delgado, J.-F. Nierengarten, N. Martín, *Nat. Chem.* **2016**, *8*, 50.
[60] M. Shoji, E. Takahashi, D. Hatakeyama, Y. Iwai, Y. Morita, R. Shirayama, N. Echigo, H. Kido, S. Nakamura, T. Mashino, T. Okutani, T. Kuzuhara, *PLoS One* **2013**, *8*, e66337.
[61] R. Klimova, S. Andreev, E. Momotyuk, N. Demidova, N. Fedorova, Y. Chernoryzh, K. Yurlov, E. Turetskiy, E. Baraboshkina, N. Shershakova, R. Simonov, A. Kushch, M. Khaitov, A. Gintsburg, *Fullerenes, Nanotubes, Carbon Nanostruct.* **2020**, *28*, 487.
[62] S. H. Friedman, D. L. DeCamp, R. P. Sijbesma, G. Srdanov, F. Wudl, G. L. Kenyon, *J. Am. Chem. Soc.* **1993**, *115*, 6506.
[63] A. Rodríguez-Fortea, S. Irle, J. M. Poblet, *Wiley Interdiscip. Rev.: Comput. Mol. Sci.* **2011**, *1*, 350.
[64] S. Bhatia, I. S. Donskyi, S. Block, C. Nie, A. Burdinski, D. Lauster, J. Radnik, A. Herrmann, R. Haag, K. Ludwig, M. Adeli, *Adv. Mater. Interfaces* **2021**, *8*, 2100285.
[65] K. H. Tan, S. Sattari, I. S. Donskyi, J. L. Cuellar-Camacho, C. Cheng, K. Schwibbert, A. Lippitz, W. E. S. Unger, A. Gorbushina, M. Adeli, R. Haag, *Nanoscale* **2018**, *10*, 9525.
[66] I. S. Donskyi, Y. Chen, P. Nickl, G. Guday, H. Qiao, K. Achazi, A. Lippitz, W. E. S. Unger, C. Böttcher, W. Chen, M. Adeli, R. Haag, *Nanoscale* **2020**, *12*, 14222.
[67] A. Faghani, I. S. Donskyi, M. Fardin Gholami, B. Ziem, A. Lippitz, W. E. S. Unger, C. Böttcher, J. P. Rabe, R. Haag, M. Adeli, *Angew. Chem., Int. Ed. Engl.* **2017**, *56*, 2675.
[68] J. Zhong, L. Song, Z. Y. Wu, S. S. Xie, M. Abbas, K. Ibrahim, H. Qian, *Carbon* **2006**, *44*, 866.
[69] L. Zhang, Z. Li, Y. Tan, G. Lolli, N. Sakulchaicharoen, F. G. Requejo, B. S. Mun, D. E. Resasco, *Chem. Mater.* **2006**, *18*, 5624.
[70] C. Ehlert, W. E. S. Unger, P. Saalfrank, *Phys. Chem. Chem. Phys* **2014**, *16*, 14083.
[71] C. Ehlert, Ph.D. Thesis, Universität Potsdam, Germany **2016**.
[72] J. Z. Jan, B. H. Huang, J. J. Lin, *Polymer* **2003**, *44*, 1003.
[73] Z. Yan, W. L. Xue, Z. X. Zeng, M. R. Gu, *Ind. Eng. Chem. Res.* **2008**, *47*, 5318.
[74] S. Bosi, T. da Ros, G. Spalluto, J. Balzarini, M. Prato, *Bioorg. Med. Chem. Lett.* **2003**, *13*, 4437.
[75] Y. Wang, Z. Tang, H. Huang, J. Li, Z. Wang, Y. Yu, C. Zhang, J. Li, H. Dai, F. Wang, T. Cai, N. Tang, *Proc. Natl. Acad. Sci. U. S. A.* **2018**, *115*, 2407.
[76] M. de Andrea, R. Ravera, D. Gioia, M. Gariglio, S. Landolfo, *Eur. J. Paediatr. Neurol.* **2002**, *6*, A41.
[77] C. Nie, P. Pouyan, D. Lauster, J. Trimpert, Y. Kerkhoff, G. P. Szekeres, M. Wallert, S. Block, A. K. Sahoo, J. Dernedde, K. Pagel, B. B. Kaufer, R. R. Netz, M. Ballauff, R. Haag, *Angew. Chem., Int. Ed. Engl.* **2021**, *60*, 15870.
[78] T. Shapira, I. Abrrey Monreal, S. P. Dion, D. W. Buchholz, B. Imbiakha, A. D. Olmstead, M. Jager, A. Désilets, G. Gao, M. Martins, T. Vandal, C. A. H Thompson, A. Chin, W. D. Rees, T. Steiner, I. Robert Nabi, E. Marsault, J. Sahler, D. G. Diel, G. R. van de Walle, A. August, G. R. Whittaker, P.-L. Boudreault, R. Leduc, H. C. Aguilar, F. Jean, *Nature* **2022**, *605*, 340.
[79] K. M. White, R. Rosales, S. Yildiz, T. Kehrer, L. Miorin, E. Moreno, S. Jangra, M. B. Uccellini, R. Rathnasinghe, L. Coughlan, C. Martinez-Romero, J. Batra, A. Rojc, M. Bouhaddou, J. M. Fabius, K. Obernier, M. Dejosez, M. J. Guillén, A. Losada, P. Avilés, M. Schotsaert, T. Zwaka, M. Vignuzzi, K. M. Shokat, N. J. Krogan, A. García-Sastre, *Science* **2021**, *371*, 926.
[80] K. Harano, A. Narita, E. Nakamura, *Chem. Lett.* **2013**, *42*, 1176.
[81] I. Donskyi, K. Achazi, V. Wycisk, C. Böttcher, M. Adeli, *Chem. Commun.* **2016**, *52*, 4373.
[82] S. Skariyachan, D. Gopal, D. Deshpande, A. Joshi, A. Uttarkar, V. Niranjan, *Infect., Genet. Evol.* **2021**, *96*, 105155.
[83] T. D. Marforio, E. J. Mattioli, F. Zerbetto, M. Calvaresi, *Molecules* **2022**, *27*, 1916.